Chemical Papers
https://doi.org/10.1007/s11696-020-01331-x

ORIGINAL PAPER

Chitosan as a coating material in enhancing the controlled release behaviour of zinc hydroxide nitrate–sodium dodecylsulphate–bispyribac nanocomposite

Sharifah N. M. Sharif[1] · Norhayati Hashim[1,2] · Illyas M. Isa[1,2] · Suriani A. Bakar[3] · Mohamad I. Saidin[1] · Mohamad S. Ahmad[1] · Mazidah Mamat[4] · Mohd Z. Hussein[5] · Rahadian Zainul[6]

Received: 26 February 2020 / Accepted: 19 August 2020

Abstract

The aim of this study is to modulate the controlled release properties of zinc hydroxide nitrate–sodium dodecylsulphate–bispyribac (ZHN–SDS–BP) nanocomposite, by coating the nanocomposite using chitosan. This study was conducted as part of an effort to reduce the environmental problems caused by the over-use of pesticides. The characterisation study shows that chitosan had been successfully coated onto the outer surface of the ZHN–SDS–BP (BP concentration of 0.05 M) without changing the types of ions intercalated in its interlayer gallery. The chitosan-coated nanocomposite, ZHN–SDS–BP–Chi also possesses a better thermal stability compared to the uncoated nanocomposite. Owing to the polycationic, hygroscopic nature, and gelation ability of chitosan, the chitosan coating was found to significantly prolong the release of bispyribac. The ZHN–SDS–BP–Chi showed a better performance in releasing pesticides, with prolonged release time ranging from 462 to 5349 min, compared to 74 to 4117 min for the uncoated nanocomposites. The release kinetic studies reveal that the release of bispyribac from the ZHN–SDS–BP–Chi is controlled by a pseudo-second-order kinetic model, thus signifying that the release mechanism is via dissolution and ion-exchange processes. The potential of chitosan in slowing the release of BP from ZHN–SDS–BP–Chi will hopefully contribute to minimise the risk of pollution resulting from the excessive use of pesticides.

Keywords Zinc hydroxide nitrate · Sodium dodecylsulphate · Bispyribac · Chitosan · Controlled release formulation

Introduction

The pesticide residues that remain on the surface and groundwater are an aftereffect of the excessive use of these substances in agriculture (Carazo-Rojas et al. 2018; Masoud et al. 2018; Skevas 2020). The leaching of the pesticide residues through the soil not only will contaminate the water, but will eventually enter the food cycle, hence, affect the living organisms in an entire population (Diendéré et al. 2018; Jin et al. 2018; Sankhla 2018; Solé et al. 2018; Toichuev et al. 2018; Bashnin et al. 2019; Mhadhbi et al. 2019). The specific harmful effect of the pesticide residues on the living organisms includes cancer, tumours, allergies and

Electronic supplementary material The online version of this article (https://doi.org/10.1007/s11696-020-01331-x) contains supplementary material, which is available to authorized users.

✉ Norhayati Hashim
norhayati.hashim@fsmt.upsi.edu.my

[1] Department of Chemistry, Faculty of Science and Mathematics, Universiti Pendidikan Sultan Idris, 35900 Tanjong Malim, Perak, Malaysia

[2] Nanotechnology Research Centre, Faculty of Science and Mathematics, Universiti Pendidikan Sultan Idris, 35900 Tanjong Malim, Perak, Malaysia

[3] Department of Physics, Faculty of Science and Mathematics, Universiti Pendidikan Sultan Idris, 35900 Tanjong Malim, Perak, Malaysia

[4] Faculty of Science and Environment Marine, Universiti Malaysia Terengganu, 21030 Kuala Terengganu, Terengganu, Malaysia

[5] Materials Synthesis and Characterization Laboratory, Institute of Advanced Technology, Universiti Putra Malaysia, 43400 Serdang, Selangor, Malaysia

[6] Department of Chemistry, Faculty of Mathematics and Natural Science, Universitas Negeri Padang, Padang, West Sumatra 25171, Indonesia

Published online: 29 August 2020

hypersensitivity, damage to the central and peripheral nervous systems, reproductive inhibition, cellular damage, and suppression of the immune and endocrine system (Sankhla 2018; Terziev and Petkova-Georgieva 2019).

Therefore, to minimise the incorporation of the pesticide residues into food and water cycle, extensive research on controlled release formulation (CRF) of agrochemicals has been reported in the previous studies (Kah and Hofmann 2014; Cao et al. 2019; Seven et al. 2019; Song et al. 2019; Tang et al. 2019; Wani et al. 2019). The pesticide with CRF was fabricated by incorporating or intercalating the pesticide into a host material which acts as a carrier for the pesticide (Bugatti et al. 2019; Rebitski et al. 2019; Sarijo et al. 2019; Wang et al. 2019). The interactions that exist between the host and the pesticide help in extending the time release of the pesticide by limiting the amount of pesticide immediately available, hence minimising undesirable transport loss (Cardoso et al. 2006). A great deal of consideration has been given to clay-based materials to be used as host materials for CRF as they are naturally abundant, non-toxic, great biocompatibility, and good ion-exchange ability (Cardoso et al. 2006; Choy et al. 2007; Radian and Mishael 2008; Mohsin et al. 2013; Chen et al. 2017; Allou et al. 2018; Bernardo et al. 2018; Nath and Dolui 2018; Bugatti et al. 2019; Rebitski et al. 2019). These amazing properties also allow the clay-based host material to be exploited not only in agricultural field, but also in numerous other fields, including medicinal, cosmetic, food technology, and sensor development (Isa et al. 2012, 2015; Wardani et al. 2014; Ahmad et al. 2018; Aziz et al. 2019; Zainul et al. 2019).

Recent developments have been reported on the possibility of combining the clay-based material with polysaccharides for various applications and one of these applications is in improving the efficacy of CRF (Fernández-Pérez et al. 2011; Korehei and Kadla 2014; Bugatti et al. 2019; Liu et al. 2019a). Some polysaccharides, chitosan, for example, may undergo certain chemical or physical crosslinked processes to increase their water solubility and gelation ability (Dong et al. 2012; Sarkar and Singh 2018; Liu et al. 2019b; Rasib et al. 2019; Song et al. 2019; Xu et al. 2019). The polysaccharide gel works as a matrix that helps in slowing the release of the pesticide, thus maintaining an effective release level of pesticide for an extended period (Harish Prashanth and Tharanathan 2007; Neri-Badang and Chakraborty 2019; Wani et al. 2019; Xu et al. 2019). Several advantages that are offered by a polysaccharide-derived polymer host material for CRF include their great biodegradability, low toxicity, mucoadhesive potential, and cost-efficiency (Dong et al. 2012; Shukla et al. 2013; Frank et al. 2017, 2020; Liu et al. 2019a). The chemical structure of chitosan is provided in Fig. 1.

This study is an extension of our recent paper which reported on the synthesis of zinc hydroxide nitrate–sodium dodecylsulphate–bispyribac (ZHN–SDS–BP) (Sharif et al. 2019). Our previous paper has revealed that ZHN is a promising host material in implementing the slow release of bispyribac (BP) herbicide. Therefore, as an endeavour to produce safer herbicide with a better efficiency, the present work is carried out to further enhance the controlled release behaviour of the ZHN–SDS–BP nanocomposite by introducing chitosan as a coating material. Due to the unique nature of chitosan, it is indeed, very intriguing to investigate the potential of this polysaccharide in prolonging the release rate of BP.

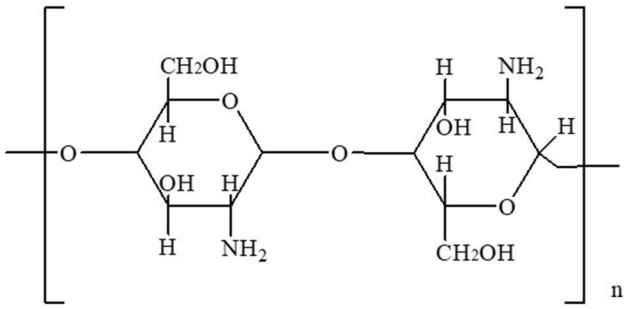

Fig. 1 The chemical structure of chitosan

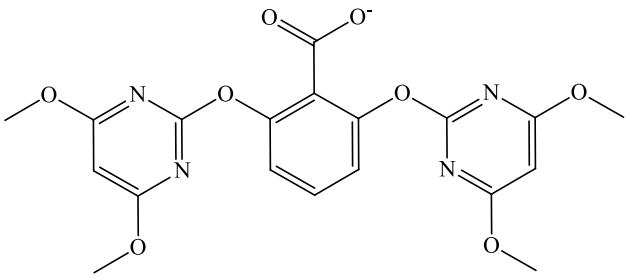

Fig. 2 The chemical structure of bispyribac

The chitosan-coated ZHN–SDS–BP nanocomposite (ZHN–SDS–BP–Chi) was analysed using various characterisation instruments, so that any changes on their physicochemical properties after the chitosan-coating process can be observed. The release behaviour and the release mechanism of BP from the ZHN–SDS–BP–Chi nanocomposite were also carried out in this study. The intercalated herbicide, BP, is a selective, post-emergence herbicide that commonly used in paddy cultivation to kill weeds, such as water hyacinth and hydrilla (Durborow 2014). The chemical structure of bispyribac is shown in Fig. 2.

Experimental

Materials

All reagents were used as received. $Zn(NO_3)_2{\cdot}6H_2O$ (98% purity) and sodium dodecylsulphate (SDS) were purchased from Systerm Chemicals. The herbicide, BP, was bought from China (purity 98%). Glacial CH_3COOH was bought from Systerm Chemicals and chitosan (≥ 75–85% deacetylated) was purchased from Sigma-Aldrich. Aqueous solutions of sodium phosphate (Na_3PO_4), sodium sulphate (Na_2SO_4), and sodium chloride (NaCl) were prepared by dissolving each salt in deionised water (0.3 M, 0.5 M, and 1.0 M).

Synthesis of ZHN–SDS–BP, ZHN–SDS–Chi, and ZHN–SDS–BP–Chi nanocomposites

ZHN–SDS and ZHN–SDS–BP were synthesised using ZHN, $Zn_5(OH)_8(NO_3)_2{\cdot}2H_2O$ via co-precipitation method as previously reported (Sharif et al. 2019). The ZHN–SDS was prepared by reacting 40 mL of 20 mmol $Zn(NO_3)_2{\cdot}6H_2O$ and 40 mL of 10 mmol SDS, under pH controlled environment (pH 6.5) and continuous flow of nitrogen. The mixture obtained was aged (at 70 °C for 24 h), collected by centrifuges (at 4000 rpm for 5 min), dried in the oven, and labelled as ZHN–SDS. The ZHN–SDS–BP was synthesised by dispersing 0.3 g ZHN–SDS into 50 mL of 2.5 mmol BP solution and stirred for 2 h. The mixture obtained was also aged (at 70 °C for 24 h), collected by centrifuges (at 4000 rpm for 5 min), and dried in the oven. The results on the characterisation studies of both ZHN–SDS and ZHN–SDS–BP have been reported in our previously published paper, and the percentage loading of BP intercalated in the interlayer gallery of ZHN–SDS–BP was found to be 61.34% (Sharif et al. 2019). The ZHN–SDS–BP was coated with chitosan at a mass ratio of 1:1. 0.1 g of chitosan was dissolved in 1% glacial CH_3COOH, diluted using deionised water (V_T = 50 mL) and stirred for 24 h until dissolved. 0.1 g ZHN–SDS–BP was dispersed into the chitosan mixture and stirred for 18 h to be coated with chitosan. The product was centrifuged (4000 rpm for 5 min) and left in an oven at 60 °C for 24 h. The dried product was ground into fine powder before it was stored in a sample bottle and labelled ZHN–SDS–BP–Chi. A similar procedure was repeated on the ZHN–SDS and the product obtained was labelled ZHN–SDS–Chi.

Characterisation

The powder X-ray diffraction (PXRD) patterns were recorded in a PANalytical X-pert Pro MPD diffractometer using CoK_α radiation (λ = 1.54056 Å). The PXRD scanning was set to an angle range of 2°–60°, 2°/min scanning speed, 9.44 s scan step time, 40 kV operating voltage, and 30 mA operating current. Fourier transform infrared (FTIR) spectroscopy was carried out using the KBr disk method on a Nicolet FTIR spectrometer, with wavenumbers ranging from 400 to 4000 cm^{-1} and a nominal resolution of 4 cm^{-1}. Thermogravimetric analysis and differential thermal analysis (TGA/DTA) were done with a Perkin Elmer Pyris 1 TGA thermo balance. The samples were put in the TGA furnace and the heating process was carried out under a nitrogen atmosphere with a heating rate of 10 °C/min from 35–1000 °C. Field emission scanning electron microscopy (FESEM) images were obtained with a Hitachi SU 8020 UHR scanning electron microscope at an accelerating voltage of 5 kV and at 10k magnification power.

Controlled release formulation study of ZHN–SDS–BP–Chi nanocomposite

BP was released from the interlayer gallery of the ZHN–SDS–BP–Chi nanocomposite using aqueous solutions of Na_3PO_4, Na_2SO_4, and NaCl, as release media. The aqueous solutions for the single system were prepared in 0.3, 0.5, and 1.0 M, whereas the binary and ternary systems were prepared in 1.0 M aqueous solutions of several combination (PO_4^{3-}–SO_4^{2-}, PO_4^{3-}–Cl^- and SO_4^{2-}–Cl^- and PO_4^{3-}–SO_4^{2-}–Cl^-). Each aqueous solution was prepared by dissolving the appropriate amount of salt in deionised water. A UV/Vis spectrometer, Lambda 25 Perkin Elmer, was used for the determination of BP. Hence, the λ_{max} value of the UV/Vis spectrometer was set to 246.4 nm. Other experimental conditions used throughout the UV/Vis spectrometer measurement are a 60 s time interval, 1.0 nm slit width, 326.0 nm lamp change, and 1.0 ordinate max 1.0 and 0.0 ordinate min. The release study was begun by adding 0.6 mg of ZHN–SDS–BP nanocomposite into a quartz cuvette containing 3.5 mL of the aqueous solution. The total concentration of BP in 0.6 mg of ZHN–SDS–BP has been predetermined using UV/Vis spectrometer, and was found to be 0.00016 M. The UV–visible spectra of the solution obtained during the predetermined step has been provided in Supplementary Material (Fig. S1). The cuvette was covered with its lid and left in the UV/Vis spectrometer until the maximum released BP was observed from the graph obtained.

Results and discussion

PXRD analysis

The PXRD patterns of chitosan, ZHN, ZHN–SDS, ZHN–SDS–Chi, ZHN–SDS–BP, and ZHN–SDS–BP–Chi

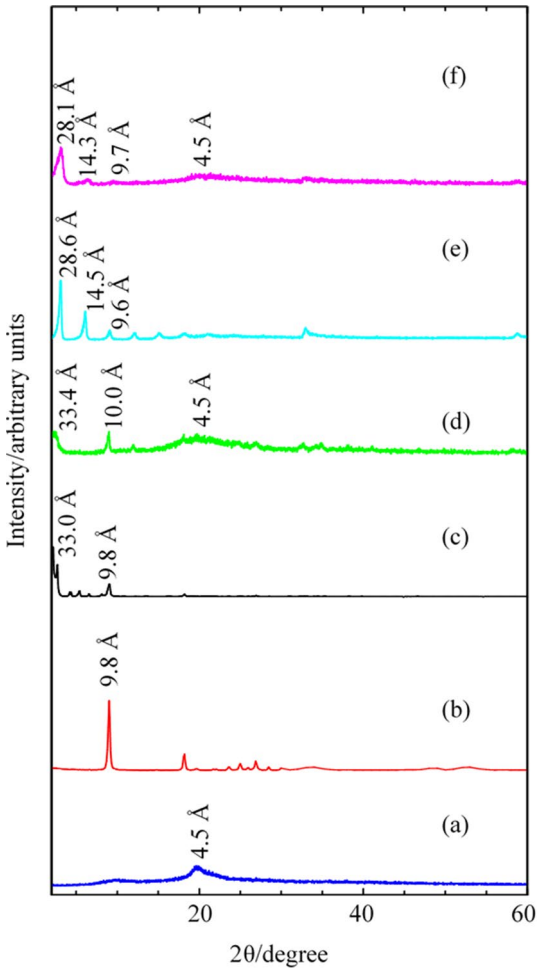

Fig. 3 PXRD patterns of **a** chitosan, **b** ZHN, **c** ZHN–SDS (Sharif et al. 2019), **d** ZHN–SDS–Chi, **e** ZHN–SDS–BP (Sharif et al. 2019), and **f** ZHN–SDS–BP–Chi

are illustrated in Fig. 3. In the diffraction pattern of ZHN, intense and sharp peak (with basal spacing of 9.8 Å) can be spotted at lower 2θ angle of the pattern, which resulting from the intercalation of NO_3^- in the interlayer gallery of the ZHN. This observation is also in a good agreement with the previous study (Yang et al. 2013). A broad, halo diffraction peak, with a basal spacing of 4.5 Å was observed in the diffraction pattern of chitosan, indicating the amorphous state of the chitosan. A similar pattern was also reported in a previous studies (Nunthanid et al. 2004; Singh et al. 2006; Salehi et al. 2010; Sanjai et al. 2014; Abbad et al. 2015; Sobh et al. 2019).

The comparisons between each diffraction pattern demonstrate that the chitosan-coating process conducted on the ZHN–SDS and ZHN–SDS–BP nanocomposites has led to some observable alterations in their diffraction peaks. The intensity of the diffraction peaks in the PXRD pattern of both ZHN–SDS–Chi and ZHN–SDS–BP–Chi was found to diminish after the chitosan-coating process. Lower intensity of both ZHN–SDS–Chi and ZHN–SDS–BP–Chi compared to their respective uncoated form indicates that the chitosan-coating process has resulted into the disordered layered structure, due to the influence of the amorphous structure of the chitosan (Zhan et al. 2003; Sobh et al. 2019). The reduction of peak intensity as a result of chitosan-coating process show good agreement with the several previous studies (Dorniani et al. 2013; Mulia et al. 2019; Pon-On et al. 2019). The PXRD analysis also reveals that the chitosan-coating process not only affect the intensity of the diffraction peaks, but also broadened the diffraction peaks. It is a known fact that the PXRD pattern could be associated with the size of crystallite, where a broader peak is commonly a result of imperfect crystals (Cho et al. 2014; Mulia et al. 2019). The disappearance of the former intense, symmetrical, sharp peaks of ZHN–SDS and ZHN–SDS–BP nanocomposite signify that the amorphous nature of chitosan has overpowered their crystalline nature and, hence, reduced their crystallinity. The diffraction peaks with a basal spacing of 4.5 Å can also be spotted in the diffraction pattern of ZHN–SDS–Chi and ZHN–SDS–BP–Chi.

It is known that the basal spacing values of the diffraction peaks reflect the height of the interlayer spacing of the nanocomposite (after consideration of several deductions). Even though significant changes were noticeable in the crystallinity of both ZHN–SDS–Chi and ZHN–SDS–BP–Chi nanocomposites, it is obvious that their basal spacings are similarly comparable to the diffraction pattern of the uncoated nanocomposites. In the diffraction pattern of ZHN–SDS, diffraction peaks appeared at 33.0 and 9.8 Å, which seems to be equivalent to the diffraction peaks of the ZHN–SDS–Chi, which appeared with basal spacings of 33.4 and 10.0 Å, respectively. As for the ZHN–SDS–BP, the diffraction peaks that appeared with a basal spacing 28.6, 14.5, and 9.6 Å are comparable to the peaks with basal spacing 28.1, 14.3, and 9.7 Å. The consistency and insignificant difference of the basal spacing values before and after undergoing chitosan coating indicate that the height of the interlayer spacing of the ZHN–SDS and ZHN–SDS–BP are similar to a certain extent. Therefore, this signifies that the ions that are intercalated in the interlayer gallery of the ZHN–SDS and ZHN–SDS–BP nanocomposites remain the same after the nanocomposites were coated. The preservation of the native structure of both ZHN–SDS and ZHN–SDS–BP nanocomposites, as reflected by their unchanged lattice parameter after the coating process is in good agreement with the previous study (Gohi et al. 2019).

Surface morphology analysis

The FESEM studies on the chitosan, ZHN, ZHN–SDS, ZHN–SDS–Chi, ZHN–SDS–BP, and ZHN–SDS–BP–Chi

demonstrate that the chitosan coating has led to some morphological changes. The FESEM images obtained are shown in Fig. 4.

The FESEM image of ZHN exhibits a flake-like structure, which is in a good agreement with the previous study (Ghotbi et al. 2012). Before undergoing the chitosan-coating process, both ZHN–SDS and ZHN–SDS–BP were also demonstrate a typical flake-like layered structure. ZHN–SDS possesses a flake-like structure with sharp edges, whereas ZHN–SDS–BP has a flake-like structure with more rounded edges (Sharif et al. 2019). The chitosan-coating process allows chitosan to be distributed on the surface of the ZHN–SDS and ZHN–SDS–BP; hence, causing the smooth and flat surface of the ZHN–SDS and ZHN–SDS–BP to become rough and uneven, which resembles the morphology of the chitosan. Chitosan also appears to enclose the whole structure of ZHN–SDS and ZHN–SDS–BP, causing both ZHN–SDS–Chi and ZHN–SDS–BP–Chi to become thicker and appear more like a clump, instead of a layer. Therefore, the results obtained from the surface morphology analysis suggested that the chitosan coating has brought obvious changes in the morphology of both ZHN–SDS–Chi and ZHN–SDS–BP–Chi nanocomposites. Similar morphology changes due to the chitosan-coating process were also reported in the previous studies (Luo et al. 2013; Rezvani and Shahbaei 2014).

Spatial arrangement of chitosan-coated ZHN–SDS–BP nanocomposite

As previously mentioned in PXRD analysis section, the basal spacing values of the diffraction are correlated to the height of the interlayer gallery. Therefore, this section will discuss in detail any changes observed in the interlayer gallery of the ZHN–SDS–BP nanocomposite after the chitosan-coating process.

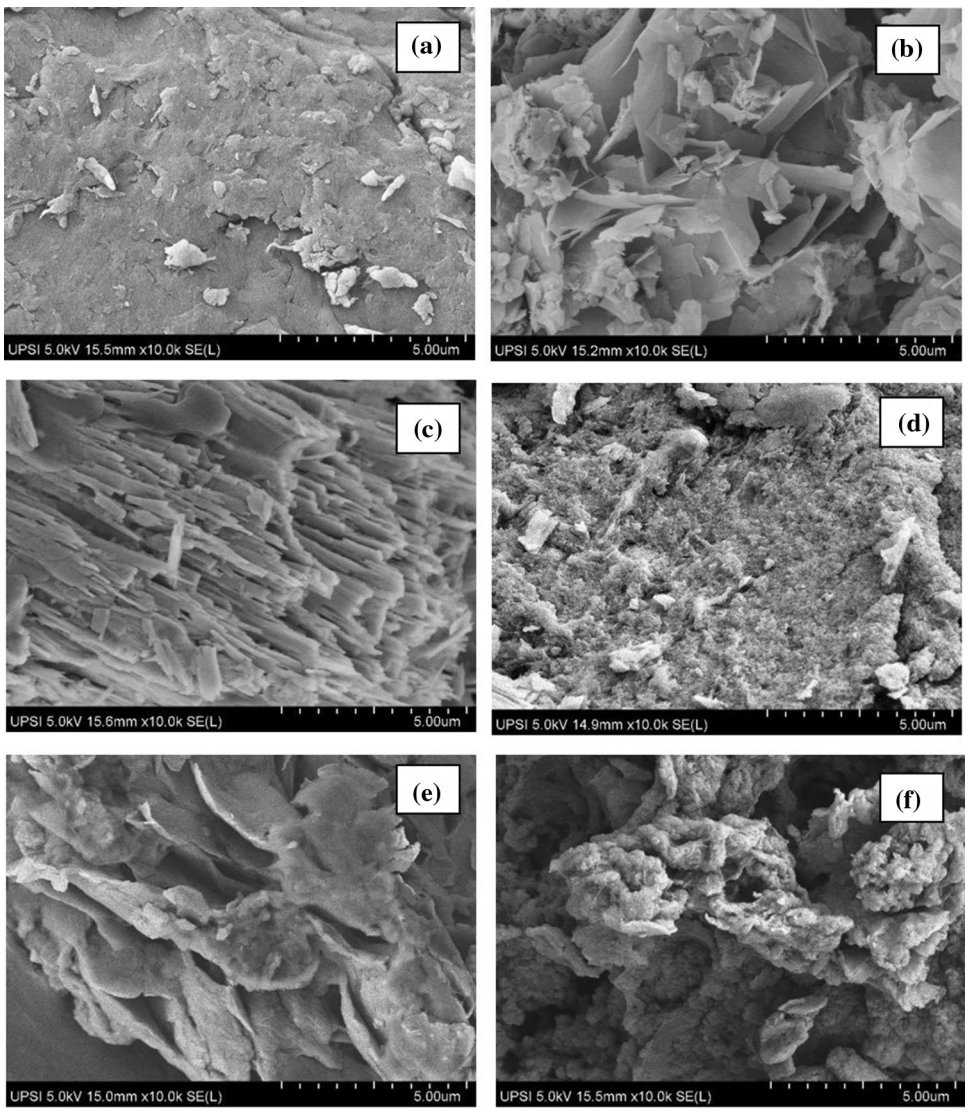

Fig. 4 Surface morphology of **a** chitosan, **b** ZHN, **c** ZHN–SDS, **d** ZHN–SDS–Chi, **e** ZHN–SDS–BP, and **f** ZHN–SDS–BP–Chi

Before the ZHN–SDS–BP nanocomposite was coated with chitosan, the SDS and BP that were intercalated in the interlayer gallery of the nanocomposite were proposed to be arranged in a monolayer (Sharif et al. 2019). The basal spacing of the intercalation peak is 28.6 Å, and hence, after considering the deduction that comes from the thickness of the ZHN layer and Zn tetrahedron, the height of the interlayer gallery of ZHN–SDS–BP is calculated to be 18.6 Å. Although the chitosan-coating process did not cause any major changes in the basal spacing values, slight differences are noticeable. The basal spacing value was reduced, from 28.6 Å to 28.1 Å, which accordingly reduced the gallery height from 18.6 to 18.1 Å (Fig. 5). The minor reduction did not reflect any changes in the type of ions intercalated in the interlayer gallery of the ZHN–SDS–BP nanocomposite, although the orientation might be slightly affected. Reduction in the ZHN–SDS–BP–Chi interlayer gallery height triggers both SDS and BP in the interlayer gallery to be arranged in a more tilted orientation while retaining their monolayer arrangement. The orientation of the SDS and BP in both ZHN–SDS–BP and ZHN–SDS–BP–Chi nanocomposites were predicted using Chem 3D Ultra 8.0 software.

FTIR analysis

The results obtained from the FTIR analysis is shown in Fig. 6. The results were also compared with the FTIR pattern of the uncoated ZHN–SDS and ZHN–SDS–BP obtained in our previous study and summarised in Table S1 in Supplementary Material (Sharif et al. 2019).

Broad peaks centred in the range of 3200–3500 cm^{-1} were observed in the FTIR spectra of ZHN–SDS, chitosan, ZHN–SDS–Chi, ZHN–SDS–BP, and ZHN–SDS–BP–Chi due to the –OH-stretching mode of the interlayer water (Hosseini et al. 2013). The existence of chitosan as a coating material was proven by the appearance of the peaks that come from the C=C-stretching vibrations of amide I and C–O–C-stretching vibrations, observed in the FTIR of ZHN–SDS–Chi at 1645 and 1057 cm^{-1} and in the FTIR of ZHN–SDS–BP–Chi at 1640 and 1041 cm^{-1}, respectively. These peaks were originally observed in the FTIR spectra of chitosan at 1665 and 1052 cm^{-1}.

The peaks that signify the asymmetric stretching of S=O from SDS can be seen in the FTIR spectra of ZHN–SDS, ZHN–SDS–Chi, ZHN–SDS–BP, and ZHN–SDS–BP–Chi at and 1217, 1218, 1178, and 1211 cm^{-1}, respectively (Qiu et al. 2009). The peaks that are attributed to the aromatic overtones of ring bonds and C=C stretching of aromatic compounds from BP can be seen in the FTIR spectra of BP at 1851 and 1583 cm^{-1}, in the FTIR spectra of ZHN–SDS–BP at 1863 and 1596 cm^{-1}, and in the FTIR spectra of ZHN–SDS–BP–Chi at 1857 and 1585 cm^{-1} (Hashim et al. 2014a). The presence of the characteristic peak of SDS in the FTIR spectra of ZHN–SDS, ZHN–SDS–Chi, ZHN–SDS–BP, and ZHN–SDS–BP, and the characteristic peaks of BP in the FTIR spectra of both ZHN–SDS–BP and ZHN–SDS–BP–Chi, are, therefore, suggestive that the intercalation of SDS and BP in the interlayer gallery of ZHN was preserved after the coating

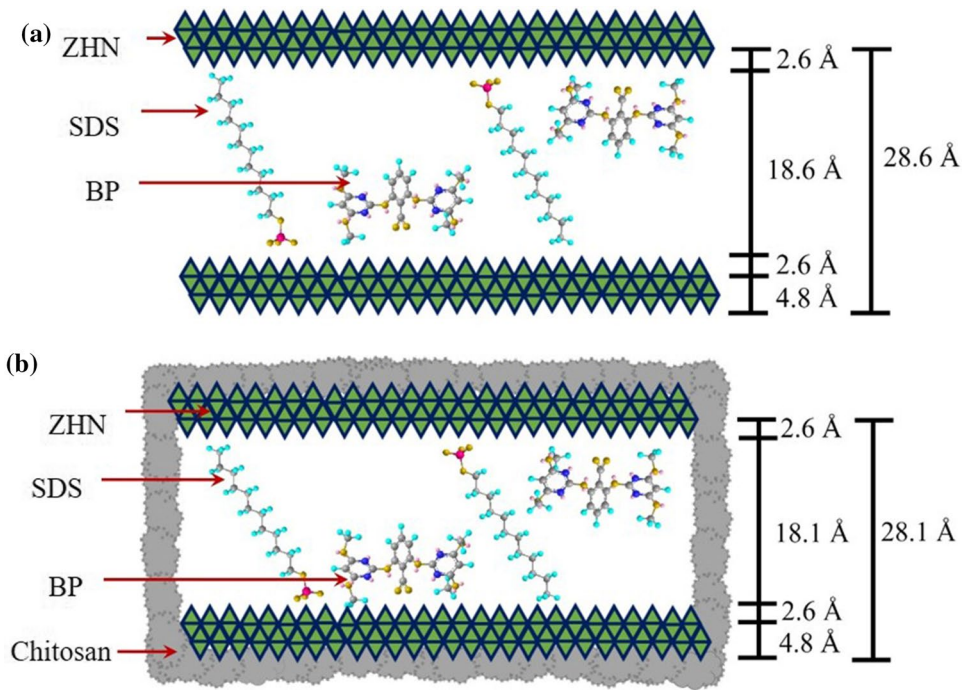

Fig. 5 Spatial orientation of BP and SDS in the interlayer gallery of **a** ZHN–SDS–BP and **b** ZHN–SDS–BP–Chi

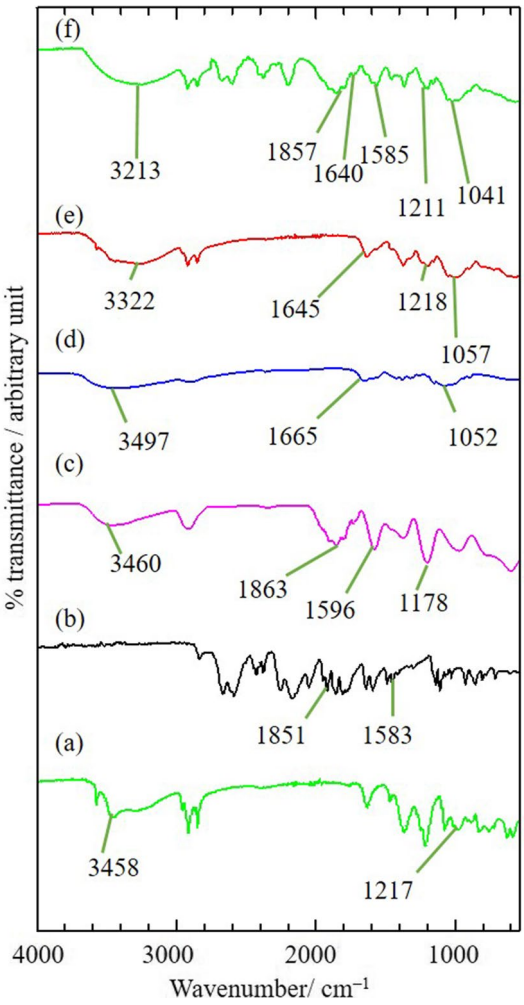

Fig. 6 FTIR spectra of **a** ZHN–SDS (Sharif et al. 2019), **b** BP (Sharif et al. 2019), **c** ZHN–SDS–BP (Sharif et al. 2019), **d** chitosan, **e** ZHN–SDS–Chi, and **f** ZHN–SDS–BP–Chi

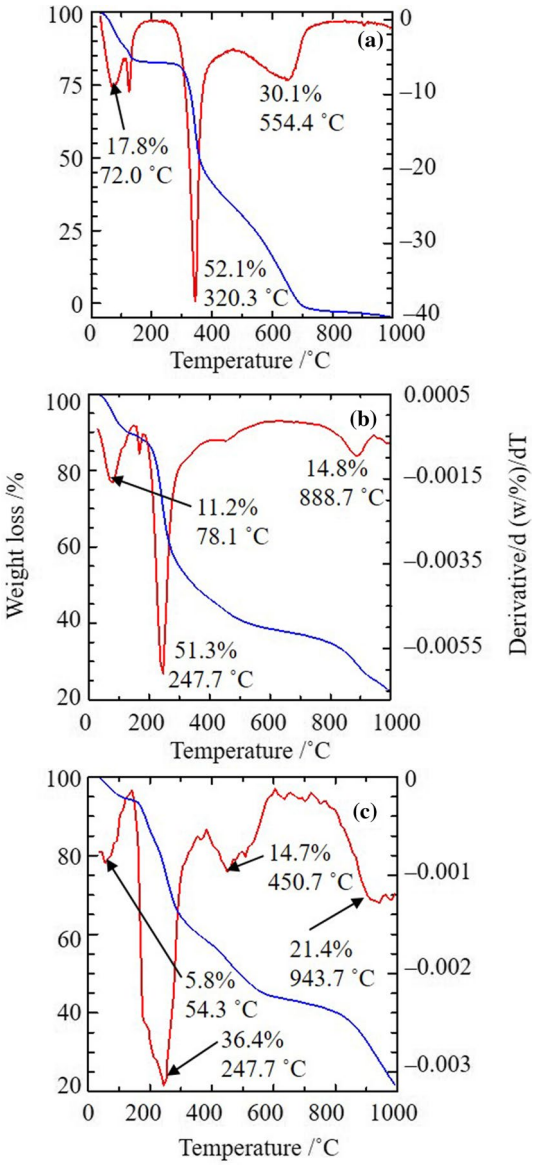

Fig. 7 TGA/DTG curves of **a** chitosan, **b** ZHN–SDS–Chi, and **c** ZHN–SDS–BP–Chi nanocomposite

process. The results obtained are in good agreement with the results from the PXRD analysis.

Thermal stability studies

The thermal stability is one of the most important aspects to be studied when investigating the physicochemical properties of a compound. Hence, in this study, the thermal stabilities of chitosan, ZHN–SDS–Chi, and ZHN–SDS–BP–Chi were investigated using TGA/DTG analysis and the results are presented in Fig. 7. The results were also compared with the thermal stabilities of the uncoated ZHN–SDS and ZHN–SDS–BP obtained in our previous study, and summarised in Table S2 in Supplementary Material (Sharif et al. 2019).

As depicted in Fig. 7, the dried chitosan had an 18.1% water content, which evaporated as the chitosan was heated to 72.0 °C. Further heating of the chitosan led to its decomposition, with 52.2% weight loss at 320.3 °C and reaching its final decomposition at 554.4 °C, with 30.2% weight loss. The thermal decomposition of ZHN–SDS involved two stages of weight loss. The first stage happened at 107.1 °C with 3.2% weight loss resulting from the elimination of adsorbed and bound water molecules; the second stage of weight loss took place at 198.2 °C with 37.2% weight loss, which is attributed to the decomposition of SDS that exists in the interlayer gallery of ZHN–SDS (Sharif et al. 2019). After the ZHN–SDS was coated with chitosan, the thermal behaviour of ZHN–SDS–Chi was notably changed. Unlike the ZHN–SDS that decomposed in two thermal events, the thermal decomposition of

ZHN–SDS–Chi occurred in three stages, at 78.1, 247.7, and 888.7 °C, with 11.2, 51.3 and 14.8% weight loss, respectively. The first stage is due to the removal of bound and adsorbed water molecules, the second stage results from the dehydration of saccharide rings and the depolymerisation of chitosan, and the last stage of decomposition occurred due to the decomposition of the SDS and the collapsing of the ZHN layer.

The comparison made in Table S2 shows that the thermal behaviour of the ZHN–SDS–BP nanocomposite also changes after the nanocomposite undergoes the chitosan-coating process. The ZHN–SDS–BP originally decomposed in three thermal events. The first thermal decomposition happened at 91.7 °C due to water molecule elimination (5.4% weight loss), the second stage occurred at 203 °C (34.8% weight loss) due to the combustion of the organic moieties that come from the intercalated BP and SDS, and the final thermal decomposition occurred at 576 °C (13.7% weight loss), as the ZHN layer collapsed (Hussein et al. 2002). As for the ZHN–SDS–BP–Chi nanocomposite, the chitosan coating causing the nanocomposite to decompose in four thermal events, which occurred at 54.3, 247.7, 450.7, and 943.7 °C, with 5.8, 36.4, 14.7, and 21.4% weight loss, respectively. The first thermal decomposition is due to the loss of adsorbed and interlayer water molecules, the second stage is due to the combustion of SDS, the third stage is due to the decomposition of the organic moieties come from the intercalated BP, and the last stage is attributed to the dehydration of saccharide rings and depolymerisation of chitosan, and also the collapse of the layered structure.

Based on the thermal stability studies, both ZHN–SDS and ZHN–SDS–BP demonstrated a similar trend of thermal behaviour changes after coated with chitosan. The chitosan coating caused an additional stage of thermal decomposition. The presence of the chitosan coating offered another protection layer on the outer surface of both ZHN–SDS and ZHN–SDS–BP, hence making the intercalated BP and SDS more protected when exposed to extreme conditions. This change is comparable with the results obtained in the TGA/DTG analysis of a previous study (Hosseini et al. 2013). An obvious increase of the temperature at which the major decomposition occurred was also observed in both ZHN–SDS and ZHN–SDS–BP after undergoing the chitosan-coating process. In the case of ZHN–SDS, the major decomposition occurred at 198.2 °C, and after it was coated with chitosan, the major decomposition happens at a higher temperature, 247.7 °C. As for the ZHN–SDS–BP, the major decomposition occurred at 203.0 °C, which then increased to 247.7 °C after the coating process. The temperature of the final decomposition is also higher in the ZHN–SDS–Chi and ZHN–SDS–BP–Chi compared to the ZHN–SDS and ZHN–SDS–BP nanocomposites. The temperatures of the final thermal decomposition of ZHN–SDS–Chi and ZHN–SDS–BP–Chi are 888.7 and 943.7 °C, whereas for the ZHN–SDS and ZHN–SDS–BP, the final thermal decomposition occurred at comparatively lower temperatures, 198.2 and 576.0 °C, respectively. Based on these findings, the thermal stability of both the ZHN–SDS and ZHN–SDS–BP nanocomposites was enhanced by the chitosan coating. These results come in a good agreement with those obtained in the previous study that also demonstrates the potential chitosan in promoting a better thermal stability of a substance (Dorniani et al. 2013).

Release study of ZHN–SDS–BP–Chi nanocomposite into various aqueous solutions

The release of BP from the ZHN–SDS–BP–Chi nanocomposite was performed in aqueous solutions of Na_3PO_4, Na_2SO_4 and NaCl prepared in concentrations of 0.3, 0.5, and 1.0 M for the single aqueous systems, and combination of PO_4^{3-}–SO_4^{2-}, PO_4^{3-}–Cl^-, and SO_4^{2-}–Cl^- for the binary aqueous solution systems and a combination of PO_4^{3-}–SO_4^{2-}–Cl^- for the ternary aqueous solution system. The release behaviour of BP was assessed based on the percentage of their accumulated release as a function of time and the release profile is shown in Fig. 8.

The release of BP from ZHN–SDS–BP–Chi in the aqueous solutions generally began with a fast release during the initial part of the release process and become slower as it approached its maximum release. Amongst the aqueous solutions, the release conducted in the aqueous solutions of NaCl was found to have the slowest release. Releasing the ZHN–SDS–BP–Chi in 0.3 M NaCl allowed the release time to be extended up to 4364 min. Although increasing the concentration of the aqueous solution of NaCl seems to shorten the release time, the release of BP from ZHN–SDS–BP–Chi in 0.5 M and 1.0 M of NaCl is still considerably prolonged, with release times of 2845 and 2662 min, respectively. When aqueous solutions of Na_2SO_4 were used as release media, the release time in 0.3, 0.5, and 1.0 M were extended to 3696, 1435, and 1258 min, respectively. As for the release in an aqueous solution of Na_3PO_4, the release time in 0.3, 0.5, and 1.0 M was prolonged to 2885, 1284, and 462 min, respectively. These observations, therefore, revealed that the release of BP from ZHN–SDS–BP–Chi in an aqueous solution of NaCl, Na_2SO_4, and Na_3PO_4 is concentration-dependent. Fewer ions, provided by lower concentration aqueous solutions, assist in slowing the release process, hence, increasing the release time.

The duration of the release of BP from the ZHN–SDS–BP–Chi also depends on the type of ions provided by the aqueous solution. The release time recorded is slowest when aqueous solutions of NaCl, which provide Cl^- anions, were used as the release media. Hence, the release time is decreasing in the order

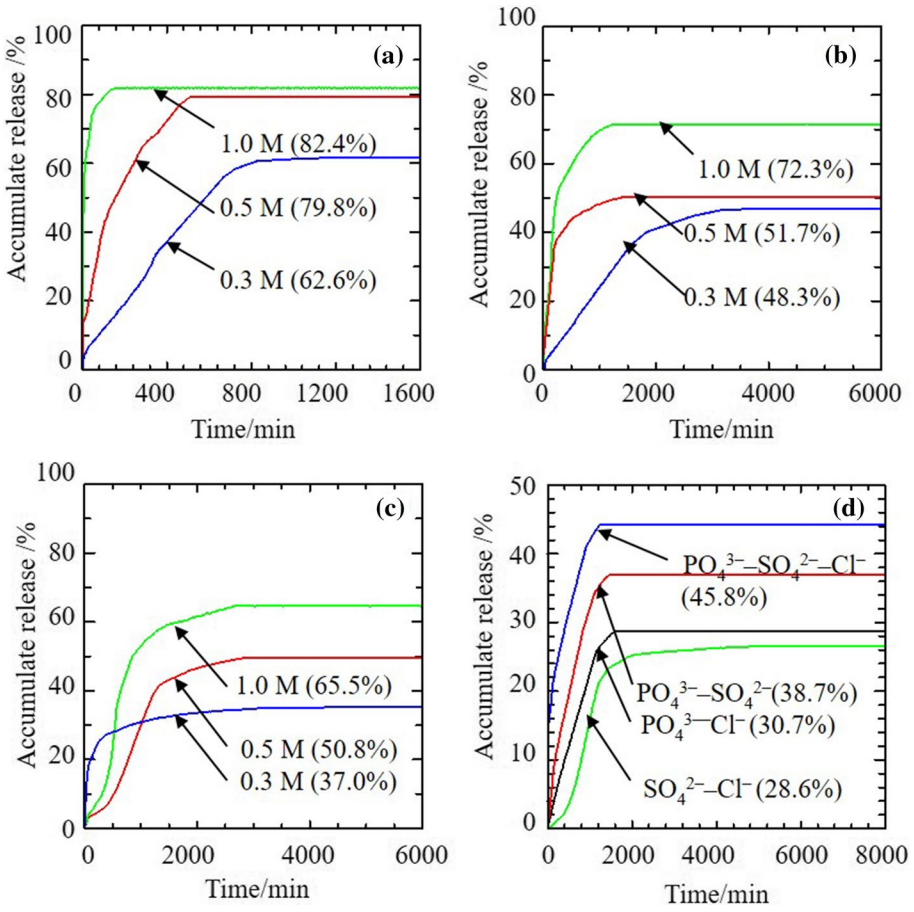

Fig. 8 Release profiles of BP from ZHN–SDS–BP–Chi nanocomposite into **a** sodium phosphate, **b** sodium sulphate, **c** sodium chloride solution in various concentration, and **d** mixture aqueous solution of phosphate, sulphate, and chloride in several combinations

of $Cl^- > SO_4^{2-} > PO_4^{3-}$. The lower affinity of monovalent Cl^- than the divalent SO_4^{2-} and trivalent PO_4^{3-} makes the Cl^- less attracted to the positively charged ZHN, therefore further prolonging the release process.

The release behaviour of BP from the ZHN–SDS–BP–Chi was also evaluated based on the maximum release percentage achieved in all aqueous solutions. Significant differences in the maximum release percentage can be observed from the release profile. The highest percentage release was obtained when the Na_3PO_4 was used as release media, 82.4%, followed by Na_2SO_4, 72.3%, and NaCl, 65.5%. The higher affinity of PO_4^{3-}, compared to the other incoming anions increased their tendency to be attracted to the ZHN, hence allowing more BP to be released into the aqueous solution. The percentage release of BP in each release media was also concentration-dependent.

The result obtained from the release of BP from the interlayer gallery of ZHN–SDS–BP–Chi nanocomposite, using binary systems of PO_4^{3-}–SO_4^{2-}, PO_4^{3-}–Cl^-, and SO_4^{2-}–Cl^- and a ternary system of PO_4^{3-}–SO_4^{2-}–Cl^- show that the release of BP in release media containing multiple types of anions is highly dependent on the composition of the incoming anion provided by the release media. This deduction is made based on the different percentages of accumulated release obtained as the release media were varied.

The release of BP in the ternary aqueous solution system allowed 45.8% of the intercalated BP to be released from the interlayer gallery of the nanocomposite within 1318 min. As for the release in the binary aqueous solution systems, 38.7, 30.7, and 28.6% of BP was released in the aqueous solutions of PO_4^{3-}–SO_4^{2-}, PO_4^{3-}–Cl^-, and SO_4^{2-}–Cl^- within 1458, 1595, and 5349 min, respectively. These results indicate that the highest percentage of accumulated release was obtained when the release process is carried out in aqueous solutions of PO_4^{3-}–SO_4^{2-}–Cl^-, and the lowest percentage was obtained when the release process is performed in aqueous solutions of SO_4^{2-}–Cl^-. The results obtained from the release study of BP in binary aqueous solution systems also revealed that the presence of trivalent PO_4^{3-} anions in the release media contributes in generating a higher accumulated release percentage due to their higher charge density and greater affinity toward the ZHN–SDS host. The presence of Cl^- anions, however, seems to lower the percentage of accumulated BP release resulting from their relatively lower charge density compared to both SO_4^{2-} and PO_4^{3-} anions.

One of the main purposes of carrying out the chitosan-coating process on the ZHN–SDS–BP nanocomposite is

to investigate the impact chitosan on the release behaviour of the ZHN–SDS–BP. Therefore, the results of the release study of ZHN–SDS–BP–Chi in various aqueous solutions were compared with the results from the release study of ZHN–SDS–BP nanocomposites that were published in our recent paper (Sharif et al. 2019). The comparisons of the percentage release and the release time of both uncoated and chitosan-coated nanocomposite are summarised in Table 1.

Based on the comparison made in Table 1, the chitosan coating has significantly extended the release time of BP from the ZHN–SDS–BP–Chi nanocomposite. There are several properties of chitosan that contribute to slowing the release of BP from the interlayer gallery of ZHN–SDS–BP–Chi. Due to the hydrophilic, hygroscopic nature and gelation ability of chitosan, chitosan is capable of forming hydrogen bonds with water molecules, hence producing a gel layer that surrounds the ZHN–SDS–BP–Chi. The gel layer works as an additional barrier that kept the BP from being immediately released into the aqueous solution, hence slowing the release process.

For the uncoated ZHN–SDS–BP, the slow release of BP is greatly contributed by the electrostatic attraction that exists between ZHN layer and the BP (Sharif et al. 2019). The electrostatic attraction not only helps in balancing the overall charge of the layer, but also assists in keeping the BP within the interlayer gallery of the nanocomposite, and allowing the sustained release of BP during the controlled release study. The zinc cation, which acts as the central metal of the ZHN layer, plays a significant role in providing the positive charge to the ZHN layer. The excessive positive charge generates by the ZHN layer allow the negatively charged carboxylate group of BP to be attracted to the positively charged ZHN layer. As for the release of BP from the ZHN–SDS–BP–Chi, the slow release is not only contributed by the excess positive charge generate by the zinc cation in the ZHN layer, but also significantly contributed by the nature of the chitosan itself. Chitosan is a type of polycationic polysaccharide, with positively charged amino groups bonded in its structure (Harding et al. 2015). Because of its polycationic nature, the positively charged amino group on the backbone of the chitosan can form electrostatic interactions with the negatively charged BP anion. The presence of chitosan on the outer surface of the ZHN–SDS–BP–Chi is, therefore, strengthened the electrostatic attraction between the ZHN layer and BP. As a result, BP is held more firmly in the interlayer gallery of the ZHN–SDS–BP–Chi and, consequently, makes it more difficult for BP to be released into the aqueous solutions. The results from the release study demonstrate the potential of chitosan coating for prolonging the release of BP from ZHN–SDS–BP–Chi. The percentage release of BP, however, decreases after the ZHN–SDS–BP was coated with chitosan. This behaviour is comparable with several previous studies (Hosseini et al. 2013; Rezvani and Shahbaei 2014; Ribeiro et al. 2014; Allou et al. 2018).

Kinetic study of BP release from the ZHN–SDS–BP–Chi nanocomposite into various aqueous solutions

Investigating the release mechanism of BP from the interlayer gallery of the ZHN–SDS–BP–Chi required fitting the release data to appropriate kinetic models. In this study, six kinetic models were employed, namely the Higuchi, zero order, first order, pseudo-second order, parabolic diffusion, and Ritger–Peppas kinetic models (Higuchi 1963; Ritger

Table 1 Comparison of the percentage release from ZHN–SDS–BP and ZHN–SDS–BP–Chi into single, binary, and ternary aqueous systems of phosphate, sulphate, and chloride

Aqueous solutions		ZHN–SDS–BP		ZHN–SDS–BP–Chi	
		Percentage release (%)	Release time (min)	Percentage release (%)	Release time (min)
Single					
PO_4^{3-}	0.3 M	72.3	1535	62.6	2885
	0.5 M	79.0	1010	79.8	1284
	1.0 M	88.2	74	82.4	462
SO_4^{2-}	0.3 M	55.9	2435	48.3	3696
	0.5 M	63.0	1224	51.7	1435
	1.0 M	75.2	1125	72.3	1258
Cl^-	0.3 M	37.8	4117	37.0	4364
	0.5 M	57.1	1326	50.8	2845
	1.0 M	71.4	1230	65.5	2662
Binary	PO_4^{3-}–SO_4^{2}	84.0	1318	38.7	1458
	PO_4^{3-}–Cl^-	83.2	1425	30.7	1595
	SO_4^{2}–Cl^-	73.1	1611	28.6	5349
Ternary	PO_4^{3-}–SO_4^{2}–Cl^-	85.4	1271	45.8	1318
Ref.		Sharif et al. (2019)		Present paper	

and Peppas 1987; Ho and Mckay 1999; Hussein et al. 2012; Bruschi 2015; Kumaresan et al. 2019). Fitting the release data for BP release from the ZHN–SDS–BP–Chi nanocomposite into aqueous solutions of Na_3PO_4, Na_2SO_4, and NaCl is presented in Figs. 9, 10, and 11. The value obtained for the model parameters, including the rate constants (k), regression values (r^2), and half-time ($t_{1/2}$), are summarised and shown in Table 2.

The pseudo-second-order kinetic model yielded the best agreement between the release data obtained experimentally and that obtained from the kinetic model. The equation used for the pseudo-second-order kinetic model is given in Eq. 1, where t represents time, M_i is the initial concentration of BP, and M_f is the final concentration of BP:

$$t/M_i = 1/M_f^2 + t/M_f. \quad (1)$$

The linearization of the release data into pseudo-second order generated the best fit, with r^2 values of $0.913 \le r^2 \le 1.00$ in aqueous Na_3PO_4 solutions, $0.962 \le r^2 \le 1.00$ in aqueous

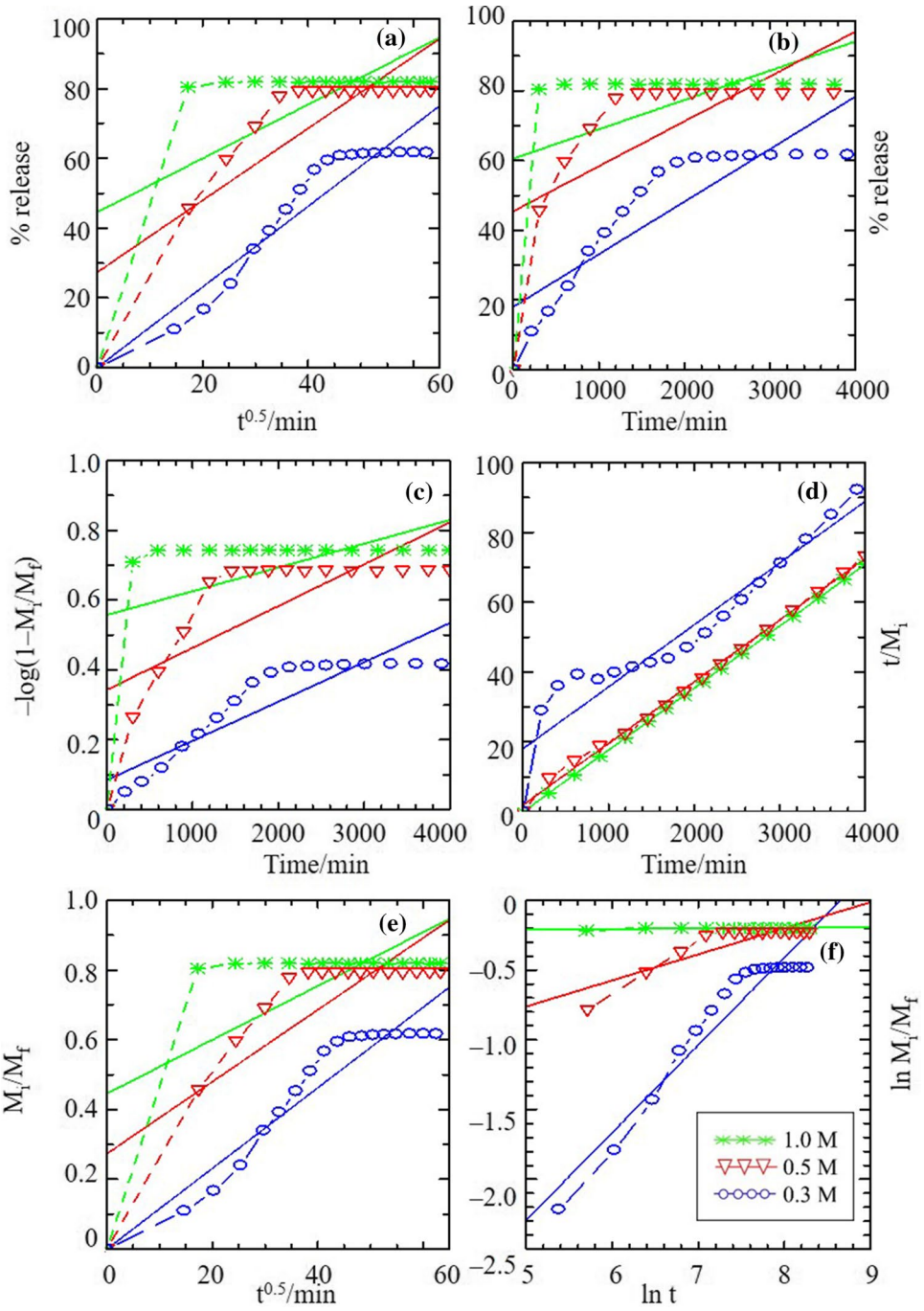

Fig. 9 Fitting the data for BP release from ZHN–SDS–BP–Chi nanocomposite into a sodium phosphate solution for the **a** Higuchi, **b** zero order, **c** first order, **d** pseudo-second order, **e** parabolic diffusion, and **f** Ritger–Peppas kinetic models

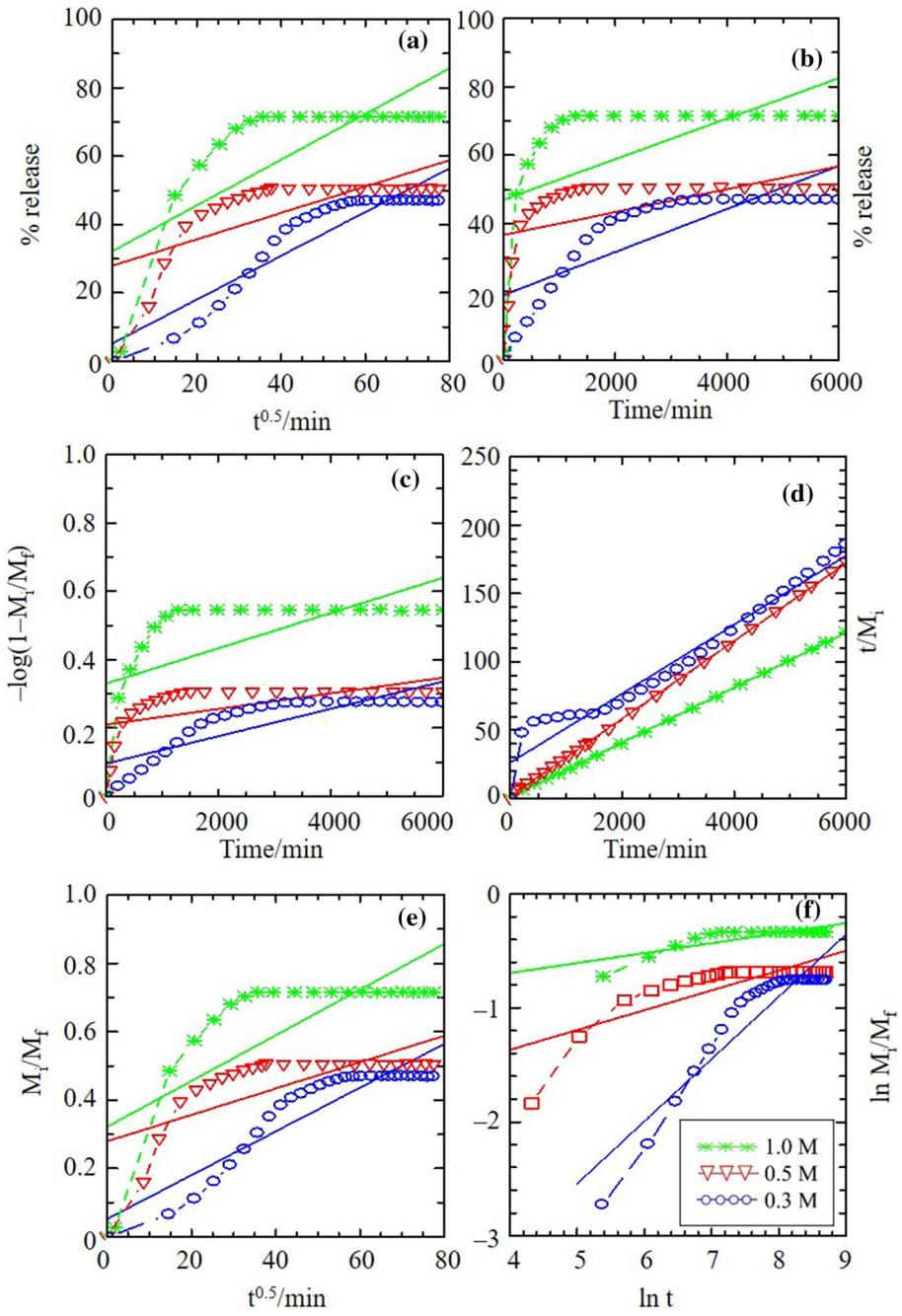

Fig. 10 Fitting the data for BP release from ZHN–SDS–BP–Chi nanocomposite into a sodium sulphate solution for the **a** Higuchi, **b** zero order, **c** first order, **d** pseudo second order, **e** parabolic diffusion, and **f** Ritger–Peppas kinetic models

Na_2SO_4 solutions, and $0.862 \leq r^2 \leq 1.00$ in aqueous NaCl solutions. Fitting the release data to other kinetic models was found to be unsatisfactory with poor r^2 values.

In the release that was governed by the pseudo-second-order kinetic model, the release mechanism of the guest ion into the release media is caused by the dissolution and ion-exchange process (Hashim et al. 2014b). These mechanisms can be related to the nature of chitosan itself. As previously stated, owing to the hydrophilic, hygroscopic nature and gelation ability of chitosan, chitosan is capable of forming a gel layer that covered the ZHN–SDS–BP–Chi nanocomposite. Exposing the chitosan gel layer to an aqueous environment for a long period hydrated the gel layer. The continuous penetration of water molecules caused the gel layer to swell and eventually led to the dissolution of the gel layer. The dissolution, therefore, allowed the BP to be slowly released into the aqueous solutions, via the ion-exchange process. The former position of BP and SDS in the interlayer gallery of ZHN–SDS–BP–Chi was then replaced with the PO_4^{3-}, SO_4^{2-}, and Cl- ions provided by the aqueous solution to counterbalance the charge of the ZHN layer.

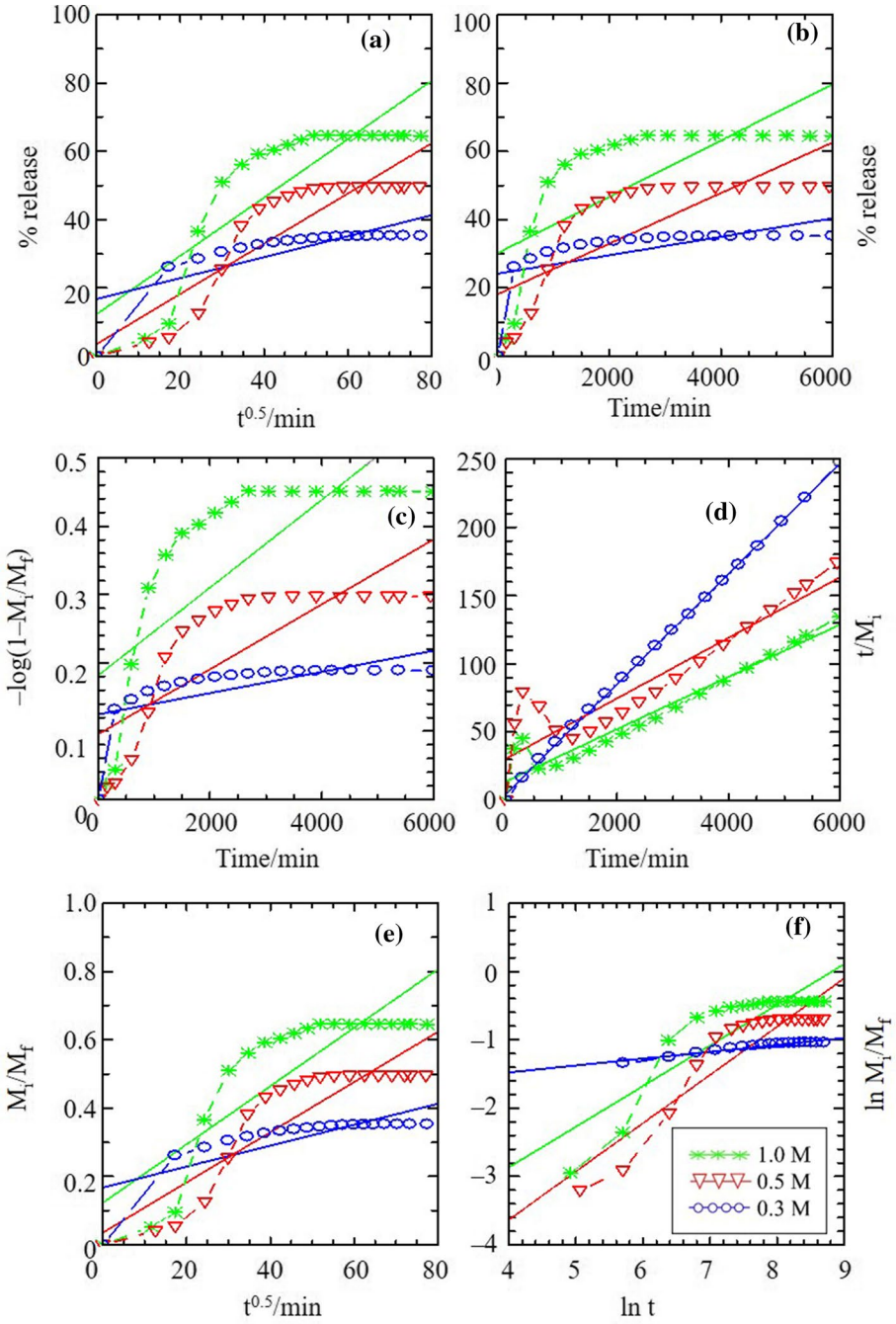

Fig. 11 Fitting of data for BP release from ZHN–SDS–BP–Chi nanocomposite into a sodium chloride solution for the **a** Higuchi, **b** zero order, **c** first order, **d** pseudo-second order, **e** parabolic diffusion and **f** Ritger–Peppas kinetic models

Conclusion

The ZHN–SDS–BP nanocomposite has been successfully coated with chitosan while preserving the ions intercalated in its interlayer gallery. The presence of SDS and BP in the interlayer gallery of ZHN–SDS–BP–Chi was confirmed using PXRD and FTIR analysis. The TGA/DTG analysis performed on the ZHN–SDS–BP–Chi revealed that the chitosan-coating process has led to significant improvement in thermal stability. The surface morphology analysis using FESEM showed that the surface morphology of the ZHN–SDS–BP–Chi nanocomposite became rough and uneven after the coating process, thus resembling the morphology of chitosan. The release study of the ZHN–SDS–BP–Chi was carried out in aqueous solutions of Na_3PO_4, Na_2SO_4, and NaCl, and the results obtained revealed that the presence of chitosan greatly prolonged the release of BP, hence, proving the potential of chitosan for enhancing the controlled release formulation of clay-based nanocomposites. The release of BP was governed by a pseudo-second-order kinetic model, which described that the release mechanism of BP occurred via a dissolution and ion-exchange process.

Table 2 Comparison of rate constants, k, and regression values, r^2, obtained from fitting the release data from ZHN–SDS–BP–Chi into aqueous solutions of Na_3PO_4, Na_2SO_4, and NaCl

Aqueous solution	Higuchi	First order	Parabolic diffusion	Ritger–Peppas	Zero order	Pseudo-second order		
	r^2	r^2	r^2	r^2	r^2	r^2	k ($\times 10^{-3}$ s^{-1})	$t_{1/2}$
Na_3PO_4								
0.3 M	0.912	0.822	0.911	0.910	0.772	0.913	0.018	829.4
0.5 M	0.714	0.545	0.715	0.762	0.470	0.997	0.062	234.8
1.0 M	0.423	0.205	0.424	0.465	0.210	1.000	0.924	15.7
Na_2SO_4								
0.3 M	0.852	0.714	0.851	0.873	0.673	0.962	0.012	1209.4
0.5 M	0.502	0.326	0.501	0.644	0.283	1.000	0.112	149.8
1.0 M	0.557	0.376	0.558	0.672	0.310	1.000	0.097	129.2
NaCl								
0.3 M	0.605	0.400	0.606	0.933	0.355	1.000	0.220	65.8
0.5 M	0.812	0.652	0.810	0.848	0.613	0.862	0.016	895.3
1.0 M	0.746	0.589	0.747	0.766	0.518	0.937	0.026	550.4

The potential of chitosan for prolonging the release of BP from ZHN–SDS–BP–Chi can help in overcoming the risk of environmental problems due to the excessive use of pesticides in paddy cultivation.

Acknowledgements This research was supported by Ministry of Education (MOE) through Fundamental Research Grant Scheme (2019-0002-102-02) and we would like to thank UPSI for all funding and support for this research.

Compliance with ethical standards

Conflict of interest The authors declare that they have no competing interest.

References

Abbad S, Zhang Z, Waddad AY, Munyendo WLL, Lv H, Zhou J (2015) Chitosan-modified cationic amino acid nanoparticles as a novel oral delivery system for insulin. J Biomed Nanotechnol 11:486–499. https://doi.org/10.1166/jbn.2015.1924

Ahmad MS, Isa IM, Hashim N, Si SM, Saidin MI (2018) A highly sensitive sensor of paracetamol based on zinc-layered hydroxide-*L*-phenylalanate-modified multiwalled carbon nanotube paste electrode. J Solid State Electrochem 22:2691–2701. https://doi.org/10.1007/s10008-018-3979-y

Allou NB, Yadav A, Pal M, Goswamee RL (2018) Biocompatible nanocomposite of carboxymethyl cellulose and functionalized carbon–norfloxacin intercalated layered double hydroxides. Carbohydr Polym 186:282–289. https://doi.org/10.1016/j.carbpol.2018.01.066

Aziz INFA, Sarijo SH, Rajidi FSM, Yahaya R, Musa M (2019) Synthesis and characterization of novel 4-aminobenzoate interleaved with zinc layered hydroxide for potential sunscreen application. J Porous Mater 26:717–722. https://doi.org/10.1007/s10934-018-0668-2

Bashnin T, Verhaert V, De Jonge M, Vanhaecke L, Teuchies J, Bervoets L (2019) Relationship between pesticide accumulation in transplanted zebra mussel (*Dreissena polymorpha*) and community structure of aquatic macroinvertebrates. Environ Pollut 252:591–598. https://doi.org/10.1016/j.envpol.2019.05.140

Bernardo MP, Guimarães GGF, Majaron VF, Ribeiro C (2018) Controlled release of phosphate from layered double hydroxide structures: dynamics in soil and application as smart fertilizer. ACS Sustain Chem Eng 6:5152–5161. https://doi.org/10.1021/acssuschemeng.7b04806

Bruschi ML (2015) Mathematical models of drug release. Strategies to modify the drug release from pharmaceutical systems. Elsevier, Amsterdam, pp 63–86. https://doi.org/10.1016/b978-0-08-100092-2.00005-9

Bugatti V, Vertuccio L, Zara S, Fancello F, Scanu B, Gorrasi G (2019) Green pesticides based on cinnamate anion incorporated in layered double hydroxides and dispersed in pectin matrix. Carbohydr Polym 209:356–362. https://doi.org/10.1016/j.carbpol.2019.01.033

Cao L, Liu Y, Xu C, Zhou Z, Zhao P, Niu S, Huang Q (2019) Biodegradable poly(3-hydroxybutyrate-*co*-4-hydroxybutyrate) microcapsules for controlled release of trifluralin with improved photostability and herbicidal activity. Mater Sci Eng C 102:134–141. https://doi.org/10.1016/j.msec.2019.04.050

Carazo-Rojas E, Pérez-Rojas G, Pérez-Villanueva M, Chinchilla-Soto C, Chin-Pampillo JS, Aguilar-Mora P, Alpízar-Marín M, Masís-Mora M, Rodríguez-Rodríguez CE, Vryzas Z (2018) Pesticide monitoring and ecotoxicological risk assessment in surface water bodies and sediments of a tropical agro-ecosystem. Environ Pollut 241:800–809. https://doi.org/10.1016/j.envpol.2018.06.020

Cardoso LP, Celis R, Cornejo J, Valim JB (2006) Layered double hydroxides as supports for the slow release of acid herbicides. J Agric Food Chem 54:5968–5975. https://doi.org/10.1021/jf061026y

Chen YX, Zhu R, Ke QF, Gao YS, Zhang CQ, Guo YP (2017) MgAl layered double hydroxide/chitosan porous scaffolds loaded with PFTα to promote bone regeneration. Nanoscale 9:6765–6776. https://doi.org/10.1039/c7nr00601b

Cho AR, Chun YG, Kim BK, Park DJ (2014) Preparation of chitosan-TPP microspheres as resveratrol carriers. J Food Sci 79:568–576. https://doi.org/10.1111/1750-3841.12395

Choy JH, Choi SJ, Oh JM, Park T (2007) Clay minerals and layered double hydroxides for novel biological applications. Appl Clay Sci 36:122–132. https://doi.org/10.1016/j.clay.2006.07.007

Diendéré A, Nguyen G, Del Corso JP, Kephaliacos C (2018) Modeling the relationship between pesticide use and farmers' beliefs about water pollution in Burkina Faso. Ecol Econ 151:114–121. https://doi.org/10.1016/j.ecolecon.2018.05.002

Dong H, Li F, Li J, Li Y (2012) Characterizations of blend gels of carboxymethylated polysaccharides and their use for the controlled release of herbicide. J Macromol Sci Part A Pure Appl Chem 49:235–241. https://doi.org/10.1080/10601325.2012.649204

Dorniani D, Bin Hussein MZ, Kura AU, Fakurazi S, Shaari AH, Ahmad Z (2013) Sustained release of prindopril erbumine from its chitosan-coated magnetic nanoparticles for biomedical applications. Int J Mol Sci 14:23639–23653. https://doi.org/10.3390/ijms141223639

Durborow RM (2014) Management of aquatic weeds. In: Chauhan BS, Mahajan G (eds) Recent advances in weed management. Springer, New York, pp 281–314

Fernández-Pérez M, Villafranca-Sánchez M, Flores-Céspedes F, Daza-Fernández I (2011) Ethylcellulose and lignin as bearer polymers in controlled release formulations of chloridazon. Carbohydr Polym 83:1672–1679. https://doi.org/10.1016/j.carbpol.2010.10.024

Frank LA, Chaves PS, D'Amore CM, Contri RV, Frank AG, Beck RCR, Pohlmann AR, Buffon A, Guterres SS (2017) The use of chitosan as cationic coating or gel vehicle for polymeric nanocapsules: increasing penetration and adhesion of imiquimod in vaginal tissue. Eur J Pharm Biopharm 114:202–212. https://doi.org/10.1016/j.ejpb.2017.01.021

Frank LA, Onzi GR, Morawski AS, Pohlmann AR, Guterres SS, Contri RV (2020) Chitosan as a coating material for nanoparticles intended for biomedical applications. React Funct Polym 147:104459. https://doi.org/10.1016/j.reactfunctpolym.2019.104459

Ghotbi MY, Bagheri N, Sadrnezhaad SK (2012) Nanocrystalline copper doped zinc oxide produced from copper doped zinc hydroxide nitrate as a layered precursor. Adv Powder Technol 23:279–283. https://doi.org/10.1016/j.apt.2011.03.007

Gohi BFCA, Zeng HY, Cao XJ, Zou KM, Shuai W, Diao Y (2019) Preparation of the hybrids of hydrotalcites and chitosan by urea method and their antimicrobial activities. Polymers. https://doi.org/10.3390/polym11101588

Harding SE, Tombs MP, Adams GG, Paulsen BS, Inngjerdingen KT, Barsett H (2015) An introduction to polysaccharide biotechnology. CRC Press, Boca Raton

Harish Prashanth KV, Tharanathan RN (2007) Chitin/chitosan: modifications and their unlimited application potential—an overview. Trends Food Sci Technol 18:117–131. https://doi.org/10.1016/j.tifs.2006.10.022

Hashim N, Hussein MZ, Isa I, Kamari A, Mohamed A, Jaafar AM, Taha H (2014a) Synthesis and controlled release of cloprop herbicides from cloprop-layered double hydroxide and cloprop-zinc-layered hydroxide nanocomposites. Open J Inorg Chem 4:1–9

Hashim N, Muda Z, Hamid SA, Isa IM, Kamari A, Mohamed A, Hussein MZ, Ghani SA (2014b) Characterization and controlled release formulation of agrochemical herbicides based on zinc-layered hydroxide-3-(4-methoxyphenyl) propionate nanocomposite. J Phys Chem Sci 1:1–6

Higuchi T (1963) Mechanism of sustained-action medication. Theoretical analysis of rate of release of solid drugs dispersed in solid matrices. J Pharm Sci 52:1145–1149. https://doi.org/10.1002/jps.2600521210

Ho YS, Mckay G (1999) Pseudo-second order model for sorption processes. Process Biochem 34:451–465

Hosseini SF, Zandi M, Rezaei M, Farahmandghavi F (2013) Two-step method for encapsulation of oregano essential oil in chitosan nanoparticles: preparation, characterization and in vitro release study. Carbohydr Polym 95:50–56. https://doi.org/10.1016/j.carbpol.2013.02.031

Hussein MZ, Yun-Hin TY, Tawang MM, Shahadan R (2002) Thermal degradation of (zinc-aluminium-layered double hydroxide-dioctyl sulphosuccinate) nanocomposite. Mater Chem Phys 74:265–271. https://doi.org/10.1016/S0254-0584(01)00481-3

Hussein MZ, Rahman NSSA, Sarijo SH, Zainal Z (2012) Synthesis of a monophasic nanohybrid for a controlled release formulation of two active agents simultaneously. Appl Clay Sci 58:60–66. https://doi.org/10.1016/j.clay.2012.01.012

Isa IM, Dahlan SNA, Hashim N, Ahmad M, Ghani SA (2012) Electrochemicals sensor for cobalt(II) by modified carbon paste electrode with Zn/Al-2(3-chlorophenoxy)propionate nanocomposite. Int J Electrochem Sci 7:7797–7808

Isa IM, Sharif SNM, Hashim N, Ghani SA (2015) Amperometric determination of nanomolar mercury(II) by layered double nanocomposite of zinc/aluminium hydroxide-3(4-methoxyphenyl)propionate modified single-walled carbon nanotube paste electrode. Ionics 3:1–10. https://doi.org/10.1007/s11581-015-1466-3

Jin S, Bluemling B, Mol APJ (2018) Mitigating land pollution through pesticide packages—the case of a collection scheme in Rural China. Sci Total Environ 622–623:502–509. https://doi.org/10.1016/j.scitotenv.2017.11.330

Kah M, Hofmann T (2014) Nanopesticide research: current trends and future priorities. Environ Int 63:224–235. https://doi.org/10.1016/j.envint.2013.11.015

Korehei R, Kadla JF (2014) Encapsulation of T4 bacteriophage in electrospun poly(ethylene oxide)/cellulose diacetate fibers. Carbohydr Polym 100:150–157. https://doi.org/10.1016/j.carbpol.2013.03.079

Kumaresan S, Pawar RR, Kevadiya BD, Bajaj HC (2019) Synthesis of saponite based nanocomposites to improve the controlled oral drug release of model drug quinine hydrochloride dihydrate. Pharmaceuticals. https://doi.org/10.3390/ph12030105

Liu B, Chen C, Wang R, Dong S, Li J, Zhang G, Cai D, Zhai S, Wu Z (2019a) Near-infrared light-responsively controlled-release herbicide using biochar as a photothermal agent. ACS Sustain Chem Eng 7:14924–14932. https://doi.org/10.1021/acssuschemeng.9b03123

Liu G, Lin G, Tan M, Zhou H, Chen H, Xu H, Zhou X (2019b) Hydrazone-linked soybean protein isolate-carboxymethyl cellulose conjugates for pH-responsive controlled release of pesticides. Polym J 51:1211–1222. https://doi.org/10.1038/s41428-019-0235-y

Luo Y, Wang TTY, Teng Z, Chen P, Sun J, Wang Q (2013) Encapsulation of indole-3-carbinol and 3,30-diindolylmethane in zein/carboxymethyl chitosan nanoparticles with controlled release property and improved stability. Food Chem 139:224–230. https://doi.org/10.1016/j.foodchem.2013.01.113

Masoud AA, Abdel-Wahab Arafa NA, El-Bouraie M (2018) Patterns and trends of the pesticide pollution of the shallow Nile Delta Aquifer (Egypt). Water Air Soil Pollut 229:148. https://doi.org/10.1007/s11270-018-3802-5

Mhadhbi T, Pringault O, Nouri H, Spinelli S, Beyrem H, Gonzalez C (2019) Evaluating polar pesticide pollution with a combined approach: a survey of agricultural practices and POCIS passive samplers in a Tunisian lagoon watershed. Environ Sci Pollut Res 26:342–361. https://doi.org/10.1007/s11356-018-3552-3

Mohsin SMN, Hussein MZ, Sarijo SH, Fakurazi S, Arulselvan P, Hin T-YY (2013) Synthesis of (cinnamate-zinc layered hydroxide) intercalation compound for sunscreen application. Chem Cent J 7:26. https://doi.org/10.1186/1752-153X-7-26

Mulia K, Chadarwati SA, Rahyussalim AJ, Krisanti EA (2019) Preparation and characterization of polyvinyl alcohol–chitosan–tripolyphosphate hydrogel for extended release of anti-tuberculosis drugs. In: International conference on informatics, technology

and engineering, 703:012010. https://doi.org/10.1088/1757-899x/703/1/012010
Nath J, Dolui SK (2018) Synthesis of carboxymethyl cellulose-g-poly(acrylic acid)/LDH hydrogel for in vitro controlled release of vitamin B12. Appl Clay Sci 155:65–73. https://doi.org/10.1016/j.clay.2018.01.004
Neri-Badang MC, Chakraborty S (2019) Carbohydrate polymers as controlled release devices for pesticides. J Carbohydr Chem 38:67–85. https://doi.org/10.1080/07328303.2019.1568449
Nunthanid J, Laungtana-Anan M, Sriamornsak P, Limmatvapirat S, Puttipipatkhachorn S, Lim LY, Khor E (2004) Characterization of chitosan acetate as a binder for sustained release tablets. J Control Release 99:15–26. https://doi.org/10.1016/j.jconrel.2004.06.008
Pon-On W, Tithito T, Maneeprakorn W, Phenrat T, Tang IM (2019) Investigation of magnetic silica with thermoresponsive chitosan coating for drug controlled release and magnetic hyperthermia application. Mater Sci Eng C 97:23–30. https://doi.org/10.1016/j.msec.2018.11.076
Qiu DP, Hou WG, Xu J, Liu J, Liu S (2009) Synthesis and characterization of imidacloprid/hydrotalcite-like compound nanohybrids. Chin J Chem 27:1879–1885. https://doi.org/10.1016/j.colsurfa.2008.11.028
Radian A, Mishael YG (2008) Characterizing and designing polycation—clay nanocomposites as a basis for imazapyr controlled release formulations. Environ Sci Technol 42:1511–1516. https://doi.org/10.1021/es7023753
Rasib SZM, Akil HM, Khan A, Hamid ZAA (2019) Controlled release studies through chitosan-based hydrogel synthesized at different polymerization stages. Int J Biol Macromol 128:531–536. https://doi.org/10.1016/j.ijbiomac.2019.01.190
Rebitski EP, Darder M, Aranda P (2019) Layered double hydroxide/sepiolite hybrid nanoarchitectures for the controlled release of herbicides. Beilstein J Nanotechnol 10:1679–1690. https://doi.org/10.3762/bjnano.10.163
Rezvani Z, Shahbaei M (2014) Bionanocomposites based on alginate and chitosan/layered double hydroxide with ciprofloxacin drug: investigation of structure and controlled release properties. Polym Compos 36:1819–1825. https://doi.org/10.1002/pc.23089
Ribeiro LNM, Alcântara ACS, Darder M, Aranda P, Araújo-Moreira FM, Ruiz-Hitzky E (2014) Pectin-coated chitosan-LDH bionanocomposite beads as potential systems for colon-targeted drug delivery. Int J Pharm 463:1–9. https://doi.org/10.1016/j.ijpharm.2013.12.035
Ritger PL, Peppas NA (1987) A simple equation for description of solute release II. Fickian and anomalous release from swellable devices. J Control Release 5:37–42
Salehi R, Arami M, Mahmoodi NM, Bahrami H, Khorramfar S (2010) Novel biocompatible composite (chitosan-zinc oxide nanoparticle): preparation, characterization and dye adsorption properties. Colloids Surf B 80:86–93. https://doi.org/10.1016/j.colsurfb.2010.05.039
Sanjai C, Kothan S, Gonil P, Saesoo S, Sajomsang W (2014) Chitosan-triphosphate nanoparticles for encapsulation of super-paramagnetic iron oxide as an MRI contrast agent. Carbohydr Polym 104:231–237. https://doi.org/10.1016/j.carbpol.2014.01.012
Sankhla MS (2018) Water contamination through pesticide & their toxic effect on human health. Int J Res Appl Sci Eng Technol 6:967–970. https://doi.org/10.22214/ijraset.2018.1146
Sarijo SH, Ahmad A, Muhsin SMN, Jubri Z (2019) Synthesis of layered organic–inorganic nanohybrid zinc–aluminium-2-(4-chlorophenoxy)-2-methyl propionic acid with controlled release properties. J Porous Mater 26:41–50. https://doi.org/10.1007/s10934-018-0605-4
Sarkar DJ, Singh A (2018) pH-triggered release of boron and thiamethoxam from boric acid crosslinked carboxymethyl cellulose hydrogel based formulations. Polym Plast Technol Eng 58:83–96. https://doi.org/10.1080/03602559.2018.1466165
Seven SA, Tastan ÖF, Tas CE, Ünal H, Ince İA, Menceloglu YZ (2019) Insecticide-releasing LLDPE films as greenhouse cover materials. Mater Today Commun 19:170–176. https://doi.org/10.1016/j.mtcomm.2019.01.015
Sharif SNM, Hashim N, Isa IM, Bakar SA, Saidin MI, Ahmad MS, Mamat M, Hussein MZ (2019) Controlled release formulation of zinc hydroxide nitrate intercalated with sodium dodecylsulphate and bispyribac anions: a novel herbicide nanocomposite for paddy cultivation. Arab J Chem 13:4513–4527. https://doi.org/10.1016/j.arabjc.2019.09.006
Shukla SK, Mishra AK, Arotiba OA, Mamba BB (2013) Chitosan-based nanomaterials: a state-of-the-art review. Int J Biol Macromol 59:46–58. https://doi.org/10.1016/j.ijbiomac.2013.04.043
Singh V, Tripathi DN, Tiwari A, Sanghi R (2006) Microwave synthesized chitosan-*graft*-poly(methylmethacrylate): an efficient Zn^{2+} ion binder. Carbohydr Polym 65:35–41. https://doi.org/10.1016/j.carbpol.2005.12.002
Skevas T (2020) Evaluating alternative policies to reduce pesticide groundwater pollution in Dutch arable farming. J Environ Plan Manag 64:733–750. https://doi.org/10.1080/09640568.2019.1606618
Sobh RA, Nasr HES, Mohamed WS (2019) Formulation and in vitro characterization of anticancer drugs encapsulated chitosan/multi-walled carbon nanotube nanocomposites. J Appl Pharm Sci 9:32–40. https://doi.org/10.7324/JAPS.2019.90805
Solé M, Bonsignore M, Rivera-Ingraham G, Freitas R (2018) Exploring alternative biomarkers of pesticide pollution in clams. Mar Pollut Bull 136:61–67. https://doi.org/10.1016/j.marpolbul.2018.08.062
Song S, Wang Y, Xie J, Sun B, Zhou N, Shen H, Shen J (2019) Carboxymethyl chitosan modified carbon nanoparticle for controlled emamectin benzoate delivery: improved solubility, pH-responsive release, and sustainable pest control. ACS Appl Mater Interfaces 11:34258–34267. https://doi.org/10.1021/acsami.9b12564
Tang C, Li Y, Pun J, Mohamed Osman AS, Tam KC (2019) Polydopamine microcapsules from cellulose nanocrystal stabilized Pickering emulsions for essential oil and pesticide encapsulation. Colloids Surf A 570:403–413. https://doi.org/10.1016/j.colsurfa.2019.03.049
Terziev V, Petkova-Georgieva S (2019) The pesticides toxic impact on the human health condition and the ecosystem. SSRN Electron J. https://doi.org/10.2139/ssrn.3477254
Toichuev RM, Zhilova LV, Makambaeva GB, Payzildaev TR, Pronk W, Bouwknegt M, Weber R (2018) Assessment and review of organochlorine pesticide pollution in Kyrgyzstan. Environ Sci Pollut Res 25:31836–31847. https://doi.org/10.1007/s11356-017-0001-7
Wang L, Yu G, Li J, Feng Y, Peng Y, Zhao X, Tang Y, Zhang Q (2019) Stretchable hydrophobic modified alginate double-network nanocomposite hydrogels for sustained release of water-insoluble pesticides. J Clean Prod 226:122–132. https://doi.org/10.1016/j.jclepro.2019.03.341
Wani TA, Masoodi FA, Baba WN, Ahmad M, Rahmanian N, Jafari SM (2019) Advances in phytonanotechnology. Elsevier Inc., Amsterdam. https://doi.org/10.1016/b978-0-12-815322-2.00012-2
Wardani NI, Isa IM, Hashim N, Ghani SA (2014) Zinc layered hydroxide-2(3-chlorophenoxy)propionate modified multi-walled carbon nanotubes paste electrode for the determination of nano-molar levels copper(II). Sens Actuators B Chem 198:243–248. https://doi.org/10.1016/j.snb.2014.03.022
Xu S, Li H, Ding H, Fan Z, Pi P, Cheng J, Wen X (2019) Allylated chitosan-poly(N-isopropylacrylamide) hydrogel based on a functionalized double network for controlled drug release. Carbohydr Polym 214:8–14. https://doi.org/10.1016/j.carbpol.2019.03.008
Yang W, Ma L, Song L, Hu Y (2013) Fabrication of thermoplastic polyester elastomer/layered zinc hydroxide nitrate nanocomposites

with enhanced thermal, mechanical and combustion properties. Mater Chem Phys 141:582–588. https://doi.org/10.1016/j.matchemphys.2013.05.074

Zainul R, Azis NA, Isa IM, Hashim N, Ahmad MS, Saidin MI, Mukdasai S (2019) Zinc/aluminium–quinclorac layered nanocomposite modified multi-walled carbon nanotube paste electrode for electrochemical determination of bisphenol A. Sensors 19:941. https://doi.org/10.3390/s19040941

Zhan L, Du Y, Zhang Z, Pang D (2003) Preparation and characterization of CdS quantum dots chitosan biocomposite. React Funct Polym 55:35–43. https://doi.org/10.1016/S1381-5148(02)00197-9